

Correspondence

Apodization and Windowing Functions

Kevin J. Parker, *Fellow, IEEE*

Abstract—In beamforming, a critical design issue is the choice of the window or apodization function. Because the transverse beam pattern at focal depth is related to the Fourier transform of the apodization function, designers must evaluate the properties of the function and its transform, jointly, to optimize the system. This paper illustrates systematic approaches to designing useful functions.

I. INTRODUCTION

WINDOW functions are well known in digital signal processing (DSP). Closely related to these are the apodization functions of sources used in imaging. In these subject areas, the objective is to choose a function that has a limited support in one domain, while also having desired properties in the transform or frequency domain. In traditional digital signal processing, there can be some flexibility in choosing the support of a window, and different applications place priorities on side-lobe levels, spectral leakage, or other measures of the transform of the window function [1]–[4].

This paper is primarily concerned with ultrasound imaging systems using focused beams produced by apodized sources. A lens or analogous time/phase shift at the source results in a transverse beam pattern across the focal region that is the Fourier transform of the source apodization function [5], [6]. The Fourier transform properties of a focused system are approximate within Fraunhofer and paraxial simplifications for a monochromatic source [5]–[7]. However, for many practical systems the relation is highly useful. For this reason, many principles in DSP concerning window functions and their transforms are pertinent to the study of ultrasound beam patterns. For example, in linear arrays, one-dimensional apodization functions can be selected and applied to the long axis of the transducer while a fixed function is applied along the shorter axis. The selection of a proper apodization function is critical to the production of an optimal beam pattern for pulse-echo imaging [8]–[11].

However, there are some important distinctions between the classical discussions of windows in DSP and the particular case of focused ultrasound apodization. DSP applications are primarily concerned with discrete samples and the discrete Fourier transform is typically utilized

with its properties of implicit periodicity. However, ultrasound pressure (or velocity) is modeled and measured in the focal region as a continuous variable [9], [12]. Even in the near field of a linear array, the array elements are typically sub-wavelength and the pressure (or velocity) can be modeled and measured as a continuous variable. Hence, for simplicity, in this paper we will be primarily concerned with continuous analytic functions and their transforms.

Furthermore, considering the specifics of ultrasound imaging systems and a range of design parameters, we highlight the following three simplified objectives:

- 1) Absolute limits on support of the apodization function. This is a practical yet inflexible constraint. Hand-held ultrasound transducers have a fixed dimension and, furthermore, the available acoustic window (for example between the ribs to view the liver) is also strictly limited in many applications.
- 2) Maximum energy transmission across the apodization function. The combination of tissue attenuation and weak scattering from organ microstructures creates a signal-starved imaging situation, and limits penetration. Furthermore, there is an upper limit to the excitation of array elements in transmission, and so any apodization function that causes the majority of elements to be set to a small amplitude—as in a slow asymptotic decay to zero—will be transmitting only a fraction of the energy that could be transmitted with a rectangular window of the same size. A similar consideration applies to the receive apodization, for which maximizing signal-to-noise is desired. This energy factor can be quantified by the integral of the square amplitude of the normalized apodization function over the support of the window.
- 3) Compact transform (narrow beamwidth for high lateral resolution). Furthermore, because ultrasound systems display a high dynamic range (typically 50 or 60 dB), side lobes are undesirable. These confound the interpretation of single versus multiple point targets and also act to fill in voids. Hence, there is a strong preference for a compact, high-resolution beam pattern without side lobes, or else side lobes well below -60 dB with rapid asymptotic decay.

As is well known from the properties of the Fourier transform, these three objectives are generally in opposition to each other. For example a rectangular window is strictly limited (Objective 1) and maximizes the transmitted energy (Objective 2), but the Fourier transform is the well-known $\sin[\omega]/\omega$ function, with side lobes as high as -13 dB with a slow asymptotic decay. Thus, this beam pattern ranks very low for Objective 3.

Because of the need to consider competing design goals, the selection of apodization or window functions and their

Manuscript received December 4, 2012; accepted March 19, 2013.

The author is with the Department of Electrical and Computer Engineering, University of Rochester, Rochester, NY (e-mail: kevin.parker@rochester.edu).

DOI <http://dx.doi.org/10.1109/TUFFC.2013.2691>

transforms requires compromises and joint optimization of the features of the functions in both domains.

This paper takes a systematic look at continuous, analytic apodization functions to illustrate trends across various functional shapes, and to identify candidates which may be optimal, considering the three objectives. The definition of Fourier transforms and functions follows the convention used in the Mathematica computational development platform (Wolfram Research, Champaign, IL), so that the results can be easily modified or expanded.

The organization of this paper is as follows: first, we examine the properties of the ideal Gaussian function and others to demonstrate how familiar functions succeed or fail to meet the objectives of high energy transmission and compact beam patterns. For background and reference, Section II examines functions that are not limited in support, and so can only be approximated in practice. Section III deals with strategies for limiting the candidate functions to a finite support, and examines the consequence of these on the Fourier transforms. Some novel functions are proposed that have useful properties and reasonably satisfy the three imaging objectives.

II. PROPERTIES OF IDEAL FUNCTIONS, WITH UNLIMITED SUPPORT

In this section, some familiar functions are examined to provide background and context for the discussions. These functions with unlimited support can demonstrate desirable or undesirable characteristics in their Fourier transforms. Strategies for limiting the support of good functions are considered later in Section III.

A. The Gaussian

The transform pair $\mathfrak{F}\{e^{-x^2/2}\} = e^{-\omega^2/2}$ illustrates that the Gaussian function is an eigenfunction of the Fourier transform operation. Lacking any side lobes, and with a strong (parabolic in log scale) asymptotic decay to zero in both domains, it would seem to be an optimal function for satisfying Objective 3 of ultrasound imaging. In fact, the well-known uncertainty principle [13] sets a lower limit on the product of the spread (Δx) of any function and the spread of its transform ($\Delta \omega$) such that

$$(\Delta x)(\Delta \omega) \geq \frac{4}{\pi}. \quad (1)$$

The Gaussian transform pair achieves the minimum value permitted by the uncertainty principle [13], in sharp comparison to many other familiar functions which can have an uncertainty product that is many times, or even orders of magnitude times the theoretical minimum. Thus, the Gaussian stands as an important reference standard. Unfortunately, it does not have limited support.

B. The Hyperbolic Secant

Another eigenfunction of the Fourier transform is the hyperbolic secant:

$$\mathfrak{F}\{\text{sech}[x]\} = \sqrt{\frac{\pi}{2}} \text{sech}\left[\frac{\pi\omega}{2}\right]. \quad (2)$$

This function and its transform are, like the Gaussian, free of unwanted side lobes. However, the asymptotic decay of $\text{sech}[x]$ goes as $\exp[-x]$, which is slow compared with the Gaussian. Hence the spread of this function and its transform are a disadvantage when considering Objectives 1 and 3 and the need for a compact waveform.

C. The Hyperbolic Secant Squared

For normalized functions (peak value = 1) that asymptotically approach zero, the rate of descent can be improved by raising the function to a power. The transform pair

$$\mathfrak{F}\{(\text{sech}[x])^2\} = \sqrt{\frac{\pi}{2}} \cdot \omega \cdot \text{csch}\left[\frac{\pi\omega}{2}\right] \quad (3)$$

yields a tighter function in the x domain, however, at the expense of a broader transform. These functions still do not decay as rapidly as the Gaussian. A comparison of these three functions is plotted in Fig. 1 for reference.

D. Flat-Topped Gaussians

In an attempt to optimize Objective 2 by extending the region of the apodization function that is near the maximum, there are several functions and modifications of the Gaussian that have more of a flat top and a wider central region. A wider central lobe function would also (generally speaking) yield a narrower Fourier transform, and hence a narrower focused beam, improving Objective 3 so long as side lobes are constrained. One strategy is to multiply the Gaussian by an increasing function:

$$\mathfrak{F}\{e^{-x^2} \cosh[x]\} = \frac{e^{-(1/4)(\omega^2-1)} \cos\left[\frac{\omega}{2}\right]}{\sqrt{2}} \quad (4)$$

or

$$\mathfrak{F}\{e^{-x^2}(1+x^2)\} = -\frac{e^{-\omega^2/4}(-6+\omega^2)}{4\sqrt{2}}. \quad (5)$$

Another strategy is to widen the transform by multiplication with a suitable function because multiplication in one domain corresponds to convolution of the transforms:

$$-\frac{1}{2}\sqrt{\frac{\pi}{2}} \text{erf}\left[\frac{-1+x}{\sqrt{2}}\right] + \frac{1}{2}\sqrt{\frac{\pi}{2}} \text{erf}\left[\frac{1+x}{\sqrt{2}}\right] = \mathfrak{F}\left\{e^{-\omega^2/2} \frac{\sin[\omega]}{\omega}\right\}. \quad (6)$$

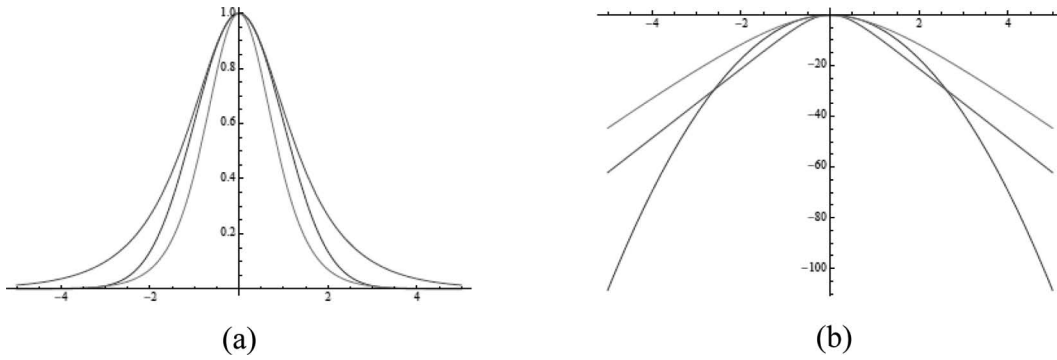


Fig. 1. Reference functions of unlimited support. (a) From outside to inside, the hyperbolic secant ($\text{sech}[x]$), the Gaussian with unity variance ($\exp[-x^2/2]$), and the hyperbolic secant squared. (b) The Fourier transforms of these functions, plotted on a decibel scale ($20\log_{10}[\text{Mag}]$) as a function of spatial frequency ω from $-5 < \omega < 5$. Because real and even functions have real and even transforms, there is no imaginary component. The widest function corresponds to the transform of the hyperbolic secant squared. The parabolic function corresponds to the Gaussian, which represents an ideal standard.

A third strategy is simply to increase the power of the exponent:

$$\begin{aligned} & \Im\{e^{-x^4/2}\} \\ &= \frac{1}{2 \times 2^{1/4}} \sqrt{\pi} \left(\frac{(\sqrt{2} \text{ hypergeometricPFQ}[\{\}, \{\frac{1}{2}, \frac{3}{4}\}, \frac{\omega^4}{128}])}{\Gamma[\frac{3}{4}]} \right) \\ & \quad - \left(\frac{(\omega^2 \text{ hypergeometricPFQ}[\{\}, \{\frac{5}{4}, \frac{3}{2}\}, \frac{\omega^4}{128}])}{\Gamma[\frac{1}{4}]} \right). \end{aligned} \quad (7)$$

These functions are plotted in Fig. 2. The general trend is that flattening the window results in oscillations (undesirable side lobe creation) in the transform.

III. FUNCTIONS OF LIMITED SUPPORT

In this section, we apply strict limits to the support of the apodization function such that $A(x)$ is specified for $-1 < x < 1$ and is 0 elsewhere. There are several strate-

gies that can be employed to enforce the limits, and each strategy has its own consequence in terms of the resulting function's Fourier transform.

A. Truncation

The simplest way of limiting a function to the span of $-1 < x < 1$ is to truncate the function at these points. This is equivalent to multiplying the function by a rectangular window. In the transform domain, this results in a convolution. Because the rectangle window has a $\text{sinc}[\omega]$ transform, the problem of multiple side lobes with slow decay is significant. Using the Gaussian as an optimal reference function, the key design parameter is the choice of the Gaussian standard deviation relative to the window size. As one example, we set σ to 0.4 so that there are 5 standard deviations within the window $-1 < x < 1$. Fig. 3 shows the side lobes produced by the truncation.

It stands to reason that as σ is decreased (and the Gaussian becomes narrower within the fixed window), the effects of truncation are minimized and the side lobe levels are reduced. However, the slope of the decay of the side lobes does not change, and the maximum energy trans-

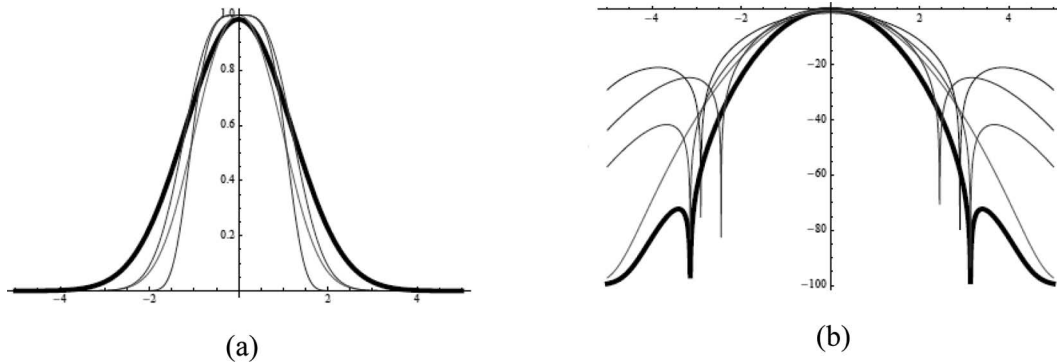


Fig. 2. In an attempt to increase the total power transmitted or received across the window, the Gaussian function is modified to produce flat-top and broadened functions. (a) $\{-1/2\sqrt{\pi/2} \text{erf}[-(1+x)/\sqrt{2}] + 1/2\sqrt{\pi/2} \text{erf}[(1+x)/\sqrt{2}]\}$, (with thick line), $\{e^{-x^2} \cosh[x]\}$, $\{e^{-x^2}(1+x^2)\}$, and $\{e^{-x^4/2}\}$ (with narrowest base). (b) The Fourier transforms of these functions for $|\omega| \leq 5$. All transforms have side lobes, meaning they oscillate at higher frequencies, with the exception of the pure Gaussian, shown again for reference (parabolic curve). The transform of the erf functions is a Gaussian times a sinc, and this function (with thick line) has the lowest side lobes of this set.

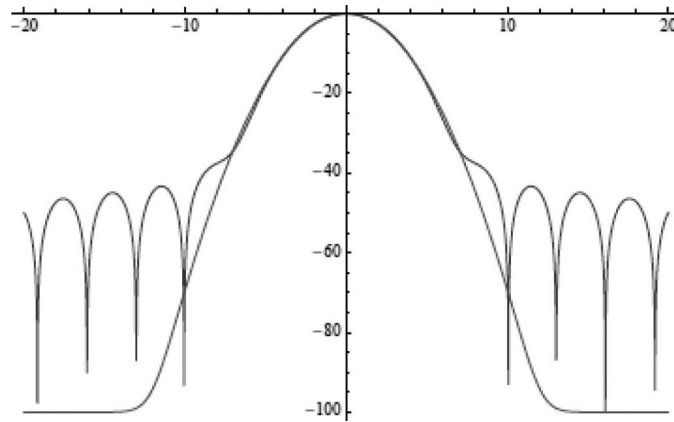


Fig. 3. The effect of abrupt truncation on the ideal Gaussian function. Shown are the transforms for $|\omega| \leq 20$ of the ideal Gaussian with a standard deviation of 0.4 units (smooth curve) and then truncated at a width of 5 standard deviations ($x = \pm 1$ units). The side lobes are seen at a level above -40 dB. These continue out to great distance. The side lobes can be further reduced by truncating the Gaussian at larger and larger standard deviations; however this has the disadvantage of setting most of the useable aperture to near zero gain.

mited (Objective 2) is decreased. Thus, this strategy is ultimately self-limiting.

B. Nonlinear Transformation of Variable

A function of unlimited support can be mapped into a limited span by replacing x with a transformation that approaches $\pm\infty$ as x approaches ± 1 . Many functions can achieve this mapping; a simple polynomial approach is

$$X = \left(\frac{x}{1 - \text{abs}[x]^\alpha} \right)^\beta \text{ for } -1 \leq x \leq 1. \quad (8)$$

If α is an even integer, the absolute value function is not necessary. The powers α and β control the rate at which larger values are mapped toward $X = \infty$. As an example, using the reference Gaussian function with the transformed variable and $\alpha = 2$, and $\beta = 1.5, 2, 3,$ and 4 are shown in Fig. 4(a). Fig. 4(b) shows a particular case where $\alpha = 8$ and $\beta = 2$, approximating a pure Gaussian. We have not found a closed-form analytical Fourier transform for this family of functions but numerical integration

of the Fourier transform integral indicates the presence of side lobes. Hence, these have no particular advantages.

C. Limited Basis Functions

Another strategy is to compose apodization functions from a set of basis functions $f_n(x)$ that approach zero at the limits, or are zero outside of $-1 < x < 1$. The popular Hann and Blackman windows are good examples using the appropriately windowed cosine function [1], [3]. In particular, the Blackman window approaches the shape of a Gaussian and correspondingly has low side lobes (below -50 dB). Fig. 5 illustrates the Blackman window using standard parameters.

The Bessel functions $J_n[x]$, where $n = 0, 1, 2, \dots$, have Fourier transforms that are strictly limited to the range $-1 < \omega < 1$, and can be expressed in terms of the function $(1 - \omega^2)$ times a Chebyshev polynomial [14]. Furthermore, the odd-order functions divided by x also have transforms that are limited to $-1 < \omega < 1$. Specifically: $J_{n+1}[x]/x$ has the transform $(1 - \omega^2)^{1/2} \cdot P_n(\omega)$, where P_n are the Legendre polynomials, and the order $(n + 1)$ is odd [15]. We take advantage of this fact by examining a linear combina-

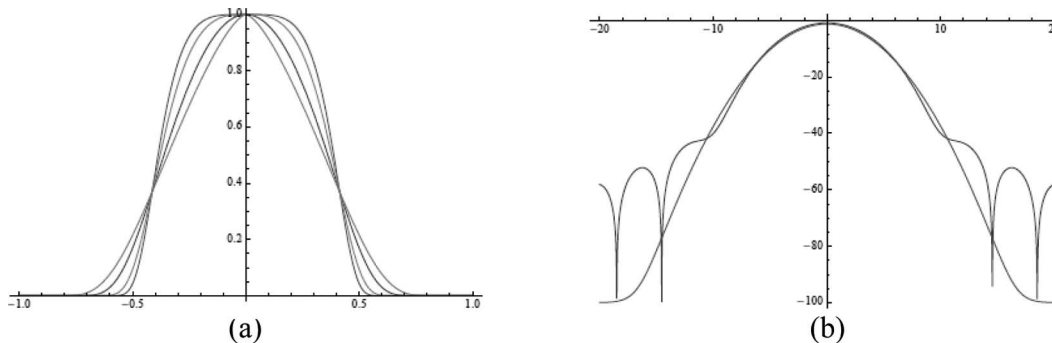


Fig. 4. Limiting the extent of functions by a nonlinear transformation of the variable. (a) Gaussian functions with x^2 (as a standard reference) and then X with different transformation parameters $\alpha = 2$ and $\beta = 1.5, 2, 3,$ and 4 . The $\beta = 1.5$ function has the widest base, whereas the $\beta = 4$ function has the narrowest base but the flattest top. (b) The transform of the standard reference Gaussian and the particular case of X derived with $\alpha = 8$ and $\beta = 2$. This latter function converges to zero smoothly at $x = 1$ but it exhibits side lobe patterns.

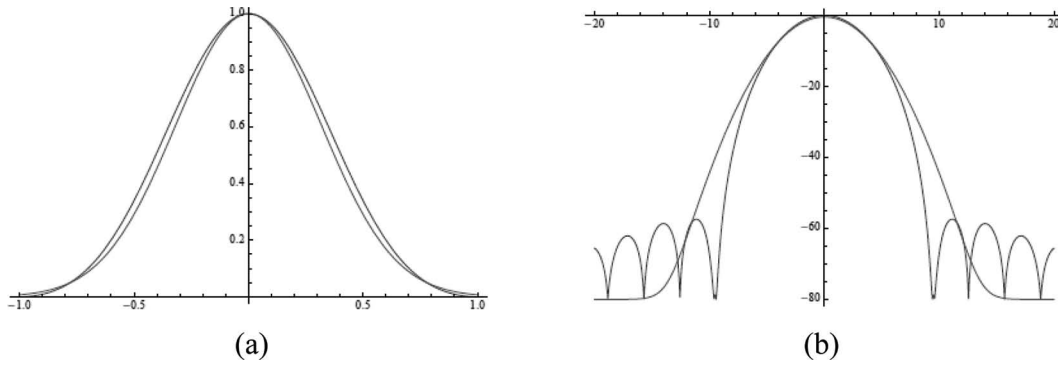


Fig. 5. The use of basis functions. (a) The standard Blackman window which uses cosine functions as basis functions, compared with a reference Gaussian of unlimited support. (b) The transform of the Blackman showing side lobes below -50 dB, but with a narrower main lobe at -40 dB compared with the Gaussian.

tion of the first 3 odd-integer orders of Bessel functions, each divided by x :

$$A(x) = J_1 \frac{x}{x} + 1.4J_3 \frac{x}{x} + 0.56J_5 \frac{x}{x}. \quad (9)$$

This function and its transform are shown in Fig. 6(a). In this case, it is the transform that is strictly limited to $-1 < \omega < 1$, and this function of ω would be used as the apodization function. These strict limits are also an example of zero mapping, described next.

D. Zero Mapping

This strategy enforces a limited support by mapping the zero (or zeroes) of a function to the points $x = \pm 1$. In general, it is helpful if the function $A(x)$, and its first and second derivatives, all approach zero at the limits. This minimizes the spread of the transform [16].

A simple polynomial function with the desired properties is the family

$$A(x) = \begin{cases} (1 - x^2)^\alpha & -1 < x < 1 \\ 0 & \text{elsewhere.} \end{cases} \quad (10)$$

As specific examples:

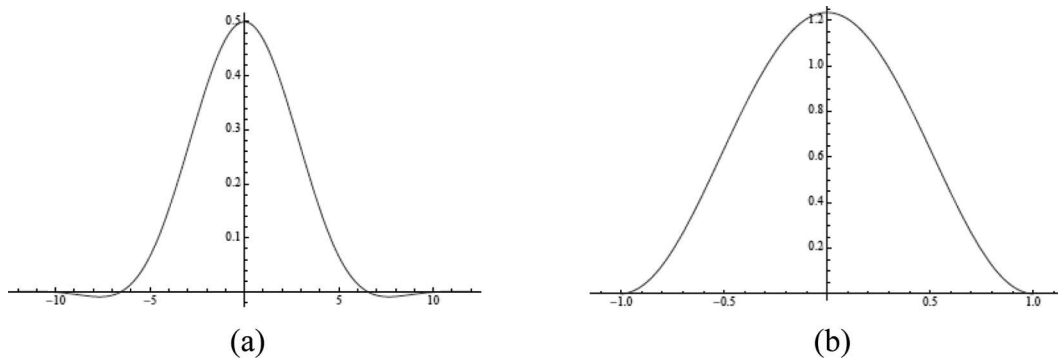


Fig. 6. The use of Bessel functions as basis functions. (a) The sum of three Bessel functions of the form $J_n[x]/x$, where n is odd. The summation is effectively zero (<0.001 or -60 dB) for $|x| > 10$. (b) The transform of (a) on a linear scale. This transform is composed of polynomials which approach zero at $\omega = \pm 1$. Specifically, $F(\omega) = 0.04(1 - \omega^2)^{1/2}[30.8 - 56.3\omega^2 + 25.5\omega^4]$ for $|\omega| \leq 1$ and 0 for $|\omega| > 1$.

$$\Im[(1 - x^2)^{1/2} \cdot (\text{UnitStep}[x + 1] - \text{UnitStep}[x - 1])] = \frac{\sqrt{\frac{\pi}{2}} \text{BesselJ}[1, \text{abs}[\omega]]}{\text{abs}[\omega]}, \quad (11)$$

$$\Im[(1 - x^2) \cdot (\text{UnitStep}[x + 1] - \text{UnitStep}[x - 1])] = \frac{2\sqrt{\frac{2}{\pi}}(-\omega \cos[\omega] + \sin[\omega])}{\omega^3}, \quad (12)$$

$$\Im[(1 - x^2)^2 \cdot (\text{UnitStep}[x + 1] - \text{UnitStep}[x - 1])] = \frac{8\sqrt{\frac{2}{\pi}}(3\omega \cos[\omega] + (-3 + \omega^2)\sin[\omega])}{\omega^5}. \quad (13)$$

Higher integer orders of α have higher order polynomials in ω , with $\cos(\omega)$ and $\sin(\omega)$. This family of functions is shown in Fig. 7. These functions have side lobes, but the levels decrease as α increases.

Another function utilizes the hyperbolic sine function:

$$A(x) = \frac{\sinh[1 - x^2]^\alpha}{\sinh[1]^\alpha}. \quad (14)$$

This function, and its first and second derivatives, approach zero as x approaches ± 1 . The Fourier transform for $\alpha = 5$ is given by a long set of erf $[a \pm i\omega]$, erfi $[a \pm i\omega]$,

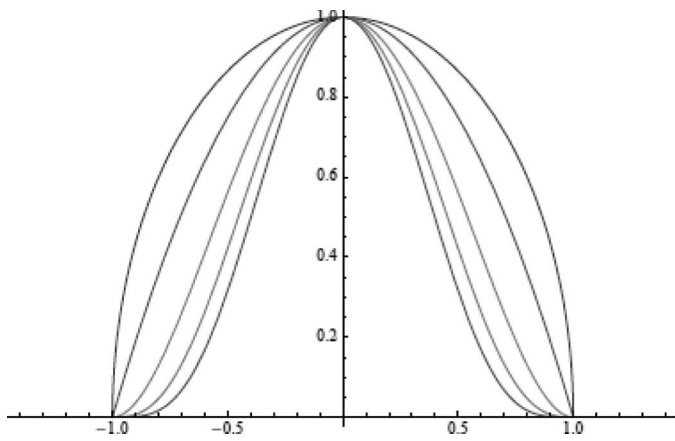


Fig. 7. The use of zero mapping. A set of functions is shown based on the polynomial $(1 - x^2)^\alpha$, from $-1 < x < 1$ and 0 elsewhere. α is shown at values of 0.5, 1, 2, 3, and 4 (narrowest curve). Their transforms have side lobes which tend to decrease as α increases.

and Gaussian terms. They appear in conjugate pairs, so the result is real and even in ω .

The results are excellent because the transform has nearly parabolic drop off on a log scale, as shown in Fig. 8, and there are no side lobes within -70 dB. In DSP applications, the corresponding N -point window would be

$$A(n) = \sinh \frac{\left[1 - \left(\frac{2n}{N} - 1\right)^2\right]^5}{\sinh[1]^5} \text{ for } n = 0 \dots (N - 1). \quad (15)$$

A related function uses a third-order polynomial approximation to the sinh function (specifically the third-order series expansion for $\sinh[x]$ evaluated at $x = 0$),

$$A(x) = \left[(1 - x^2) + \frac{(1 - x^2)^3}{6} \right]^5, \quad (16)$$

and also produces an excellent result, as shown in Fig. 9.

Furthermore, to a reasonable approximation (absolute error less than 0.4% over the interval $0 < |\omega| < 14.2$ and side lobes below -70 dB for $|\omega| > 14.2$), the \sinh^5 function emerges as an approximate eigenfunction of the Fourier transform operation, with limited support in both domains:

$$\Im \left\{ \frac{\sinh[1 - x^2]^5}{\sinh[1]^5} \right\} \cong 0.2118 \cdot \frac{\sinh\left[1 - \left(\frac{\omega}{14.2}\right)^2\right]^5}{\sinh[1]^5} \quad (17)$$

$$\begin{array}{ll} -1 \leq x \leq 1 & -14.2 < \omega < 14.2 \\ 0 \text{ elsewhere} & \varepsilon \rightarrow 0 \text{ elsewhere.} \end{array}$$

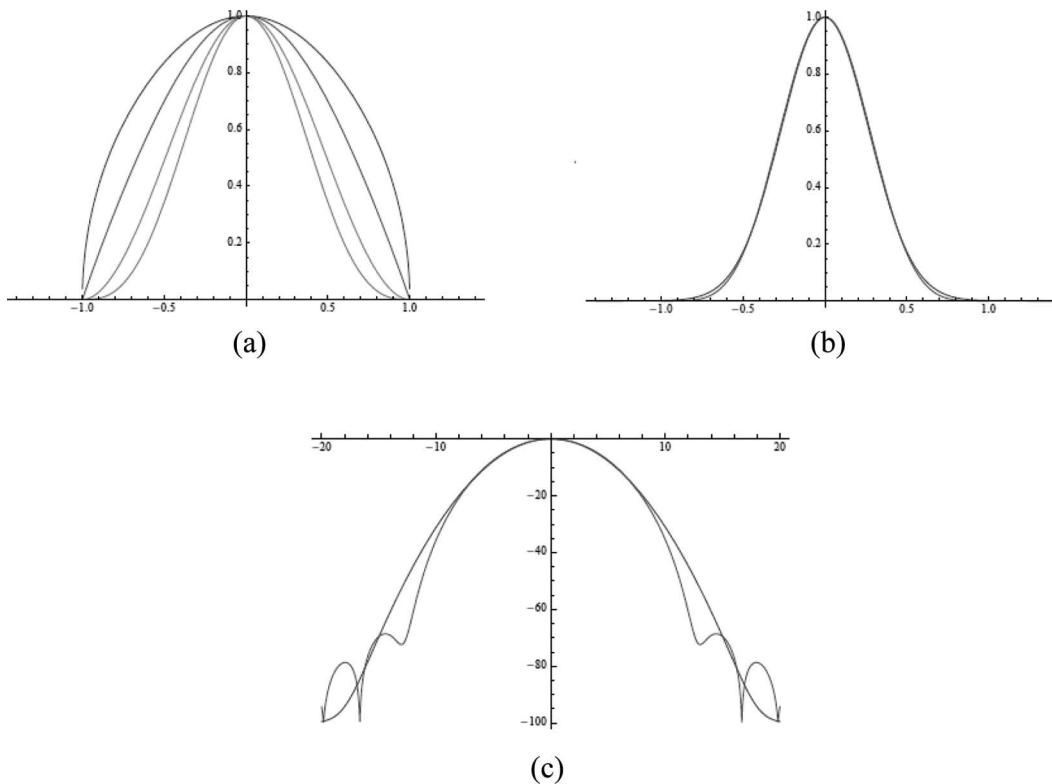


Fig. 8. The use of zero mapping with the hyperbolic sine function of argument $(1 - x^2)$ from $-1 < x < 1$ and 0 elsewhere. (a) This function is raised to the powers of 0.5, 1, 2, and 3. (b) This function raised to the fifth power, as a good approximation to a reference Gaussian (also shown), however the \sinh^5 function has strict convergence to zero at the limits $x = \pm 1$. (c) The transform of the $\sinh(1 - x^2)^5$ function, compared with the transform of a reference Gaussian. There are no side lobes in this transform within -70 dB.

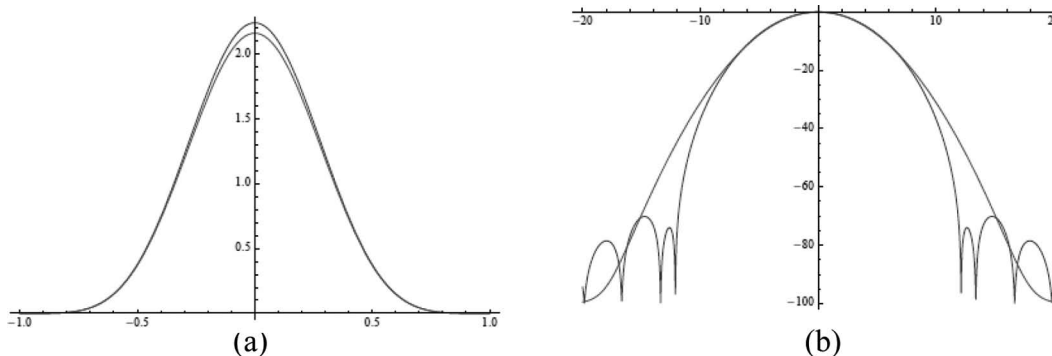


Fig. 9. A polynomial approximation to the hyperbolic sine function. (a) The \sinh^5 and its third-order polynomial approximation. (b) The transform of the third-order polynomial function, and a reference Gaussian transform.

Of course, the fundamental uncertainty limit on Fourier transform pairs makes it impossible to have strictly limited, compact support in both domains, yet with reasonable (-70 dB) approximation, this is practically achieved with these functions.

Finally, it should be noted that other monotonically increasing functions can be modified by zero mapping, for example the function $[1 - \cosh[1 - x^2]]^\alpha$ produces similar results to those previously mentioned in this section.

IV. DISCUSSION

The choice of an optimal apodization function will be dependent on the precise objectives that a designer uses, and how the objectives are weighted. Without these, we can only state some general considerations. The issue of side lobes and resolution are major concerns in high-dynamic-range medical ultrasound systems, and therefore the Gaussian function of unlimited extent is an excellent example function in that it lacks side lobes and has parabolic decay in log-magnitude space. Correspondingly, it achieves the lowest theoretical spread (uncertainty product) in both domains.

Unfortunately, practical systems cannot use this ideal function because there is a strict limit on support of the apodization function. In that case, a truncated Gaussian or a Blackman window are two common choices. These possess unwanted side lobes, although the side lobe amplitudes can be set below -50 or lower by adjusting parameters, however at greater loss in the total energy at the aperture. We have shown that, additionally, the function $A(x) = (\sinh[1 - x^2]^5)/(\sinh[1]^5)$ and its poly-

nomial approximation are advantageous in the sense that these functions and their first two derivatives approach zero at the limits of $x = \pm 1$, and correspondingly have a transform magnitude of approximately the same \sinh^5 form with nearly parabolic (in log scale) drop off with no side lobes within -70 dB. Table I summarizes some of the tradeoffs, using a few of the functions for comparison. The particular choice of beamwidth (i.e., -6 dB, -20 dB, or other) is up to the designer and some relative rankings depend on the level specified.

One way to appreciate the combination of factors is to examine the image produced from a pair of reflectors separated by a small distance. Fig. 10(a) is shows the image of two point reflectors separated by 4.68 mm laterally, at the focus of a 5 -MHz, f-number 3.2 simulated imaging system using the Field II acoustic pressure field simulation package [17]. In Fig. 10(a), a rect or uniform apodization function is used for both transmit and receive; hence the sinc side-lobe pattern is strongly visible on a 100 dB dynamic range gray scale. Fig. 10(b) shows the same reflectors and settings; however a \sinh^5 apodization pattern is used for both transmit and receive. This function has its zeroes mapped to ± 1.2 , but is truncated at ± 1 . This focal pattern has no visible side lobes but is larger than the main lobe of the sinc function. Of course, one could use a rect on transmit and receive and a \sinh^5 on receive (or other choices) to adjust the criteria in stages. Finally, a 5σ truncated Gaussian apodization is used in Fig. 10(c) in both transmit and receive modes. The truncation results in low-level side lobes.

It must be noted that the full details of beamforming in phased array systems are complex and include several factors beyond the scope of this paper. For instance, in prac-

TABLE I. EVALUATION OF SELECTED APODIZATION FUNCTIONS.

	Criteria 1 Limited support	Criteria 2 Energy (% of maximum)	Criteria 3 -6 -dB beamwidth (normalized units)	Criteria 3 Side lobe maximum level (dB)
Rect	Yes	100	3.8	-13
Gauss 5σ	By truncation	70	6.0	-43
Blackman	Yes	60	7.2	-57
Sinh ⁵	Yes	48	8.6	-78

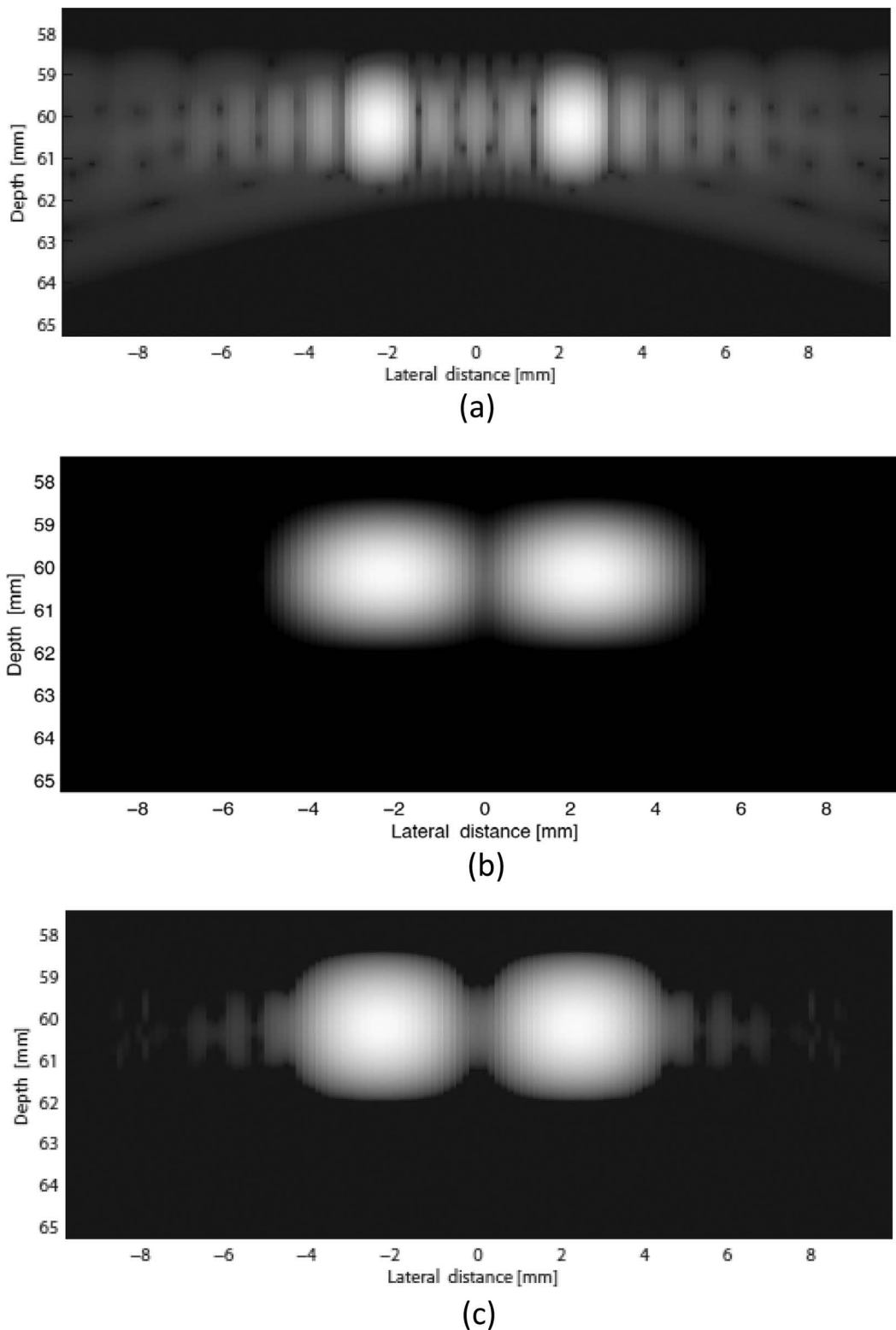


Fig. 10. Simulated images from a 5-MHz, f-number 3.2 simulated scanner using Field II and a pair of scatterers at the focus, 60 mm depth and 4.68 mm separation laterally. In the simulation, the transducer had 129 active elements and a narrowband pulse (-6 -dB bandwidth of 20%) was transmitted. (a) A flat or rect apodization was utilized for both transmit and receive. (b) A \sinh^5 apodization function was employed for both transmit and receive. The \sinh^5 apodization has no side lobes but has a wider main lobe as compared with (a). (c) A Gaussian 5σ truncated apodization is employed. This function has a narrower main lobe than the \sinh^5 but low-level side lobes as a result of truncation. Images are 100 dB dynamic range scale so that one-way side lobes down to -50 dB can be visualized.

tice, the array elements are discrete and have a form factor. Thus, a more careful modeling of the source includes a convolution of discrete sources with a representative element [5], [7], [9], [18]. Furthermore, the use of beams over many centimeters of tissue depth requires consideration of the extended beam pattern, including depth of field, f-number, focal gain, pulse bandwidth, tissue properties, and use of dynamic receive strategies [18], [19]. Other types of beams, including the limited diffraction beams such as Bessel, X-, and Axicon beams [19] can also be considered as alternatives. Finally, the issue of contrast and resolution in ultrasound systems is complex. Visualizing small voids such as cysts in tissue is critically important in clinical ultrasound, and a careful treatment of this as a function of the beam pattern requires integration over partial volumes [11], and cannot be simply extrapolated from one or two parameters in Table I.

V. CONCLUSION

The design of focused systems includes the joint optimization of conflicting requirements of the apodization function and its Fourier transform (as embodied in the lateral beam pattern at the focus). Several approaches can be taken to jointly optimize the requirements for the apodization function and the beam pattern. The most fruitful of these include: the use of basis functions, including cosine and Bessel functions, and the use of zero mapping. With these, it is possible to achieve a strictly limited support of the apodization and an approximately limited support (side lobes below -70 dB) of a compact focal beam pattern.

ACKNOWLEDGMENT

Expert assistance from S. Chen is gratefully acknowledged.

REFERENCES

- [1] F. J. Harris, "On the use of windows for harmonic analysis with the discrete Fourier transform," *Proc. IEEE*, vol. 66, no. 1, pp. 51–83, 1978.
- [2] A. V. Oppenheim and R. W. Schaffer, *Digital Signal Processing*. Englewood Cliffs, NJ: Prentice-Hall, 1975.
- [3] J. H. McClellan, R. W. Schaffer, and M. A. Yoder, *DSP First: A Multimedia Approach*. Upper Saddle River, NJ: Prentice Hall, 1998.
- [4] A. Nuttall, "Some windows with very good sidelobe behavior," *IEEE Trans. Acoust. Speech Signal Process.*, vol. 29, no. 1, pp. 84–91, 1981.
- [5] A. Macovski, *Medical Imaging Systems*. (Prentice-Hall information and system sciences series), Englewood Cliffs, NJ: Prentice-Hall, 1983, pp. 173–203.
- [6] J. W. Goodman, *Introduction to Fourier Optics*. (McGraw-Hill physical and quantum electronics series), Englewood, CO: Roberts & Co., 2005, pp. 97–126.
- [7] R. S. C. Cobbold, *Foundations of Biomedical Ultrasound*. (Biomedical engineering series), New York, NY: Oxford University Press, 2007, pp. 413–491.
- [8] C. M. W. Daft, and W. E. Engeler, "Windowing of wide-band ultrasound transducers," in *Proc. IEEE Ultrasonics Symp.*, 1996, vol. 2, pp. 1541–1544.
- [9] J. A. Jensen and N. B. Svendsen, "Calculation of pressure fields from arbitrarily shaped, apodized, and excited ultrasound transducers," *IEEE Trans. Ultrason. Ferroelectr. Freq. Control*, vol. 39, no. 2, pp. 262–267, 1992.
- [10] D. A. Guenther and W. F. Walker, "Optimal apodization design for medical ultrasound using constrained least squares, Part I: Theory," *IEEE Trans. Ultrason. Ferroelectr. Freq. Control*, vol. 54, no. 2, pp. 332–342, 2007.
- [11] D. Vilkomerson, J. Greenleaf, and V. Dutt, "Towards a resolution metric for medical ultrasonic imaging," in *Proc. IEEE Ultrasonics Symp.*, 1995, vol. 2, pp. 1405–1410.
- [12] R. S. C. Cobbold, *Foundations of Biomedical Ultrasound*. New York, NY: Oxford University Press, 2007.
- [13] R. N. Bracewell, *The Fourier Transform and its Applications*, 1st ed., New York: McGraw-Hill, 1965, p. 163.
- [14] A. Erdélyi and H. Bateman, *Tables of Integral Transforms*. vol. 1, McGraw-Hill: New York, 1954, pp. 43, 99.
- [15] A. Erdélyi and H. Bateman, *Tables of Integral Transforms*. vol. 1, New York, NY: McGraw-Hill, 1954, p. 123.
- [16] R. N. Bracewell, *The Fourier Transform and its Applications*, 1st ed., New York, NY: McGraw-Hill, 1965, pp. 135–176.
- [17] J. A. Jensen, "Simulation of advanced ultrasound systems using Field II," in *IEEE Int. Symp. Biomedical Imaging: Nano to Macro*, 2004, pp. 636–639, vol. 1.
- [18] T. L. Szabo, *Diagnostic Ultrasound Imaging: Inside Out*. (Academic Press series in biomedical engineering), Burlington, MA: Elsevier Academic Press, 2004, pp. 171–212.
- [19] J. Y. Lu, H. Zou, and J. F. Greenleaf, "Biomedical ultrasound beam forming," *Ultrasound Med. Biol.*, vol. 20, no. 5, pp. 403–428, 1994.